JOURNAL OF THERMOPHYSICS AND HEAT TRANSFER
Vol. 10, No. 1, January–March 1996

# Moving Gas Front Effects on Heat Pipe Transient Behavior

Jay H. Chung*
*Tayco Engineering, Inc., Cypress, California 90630*
and
Donald K. Edwards†
*University of California, Irvine, Irvine, California 92717*

**Axial temperature profile changes are derived for moving gas–vapor fronts in gas-controlled heat pipes and are incorporated into an engineering model of heat pipe transient behavior. Experimental data obtained with a 1.43-m- (56.3-in.-) long ammonia-filled, slab-wicked, circumferentially grooved stainless steel heat pipe with an actively controlled gas reservoir are compared to the analytical temperature profiles and temperature–time histories during startup transients. Motion of the gas front during a transient is shown to have a large effect upon the axial temperature profile, and the resulting effect upon axial conduction is a significant factor in heat pipe transient modeling.**

## Nomenclature

$A$ = cross-sectional area, m$^2$
$A_c$ = cross-sectional area of condenser, m$^2$
$b_c$ = thickness of cork plate, m
$b_e$ = thickness of heater plate, m
$C$ = thermal capacitance, J/K
$c$ = specific heat, J/kg·K
$k$ = thermal conductivity, W/m·K
$L$ = characteristic length, m
$L_b$ = length of gas-blocked condenser, m
$L_e$ = length of evaporator, m
$P$ = perimeter, m
$Pe$ = Peclet number
$Pr$ = Prandtl number
$Q$ = heat transfer rate out of active length, W
$Q_e$ = heat input rate at evaporator, W
$Re$ = Reynolds number
$T$ = temperature, K
$T_e$ = evaporator temperature, K
$T_s$ = sink temperature, K
$t$ = time, s
$U$ = overall heat transfer coefficient, W/m$^2$·K
$v$ = velocity, m/s
$W_c$ = width of condenser saddle, m
$W_e$ = width of evaporator saddle, m
$\rho$ = mass density, kg/m$^3$

## Introduction

HEAT pipes can transport heat with only a small temperature drop and the operating temperature varies according to the heat input and heat sink condition. Such plain or simple heat pipes are said to be fixed conductance pipes.[1,2] In many cases, it is desired to maintain the heat source temperature at an almost constant level over a wide range of heat input and heat sink conditions. This source temperature stabilization can be achieved by using a gas-loaded variable conductance heat pipe (VCHP).[3,4] The heat pipe is connected to a reservoir having a volume much larger than that of the heat pipe vapor space. The reservoir is filled with a noncondensable inert gas. On applying heat to the evaporator section, the vapor will push the inert gas back toward the reservoir and a vapor–gas interface will be created at some point in the condenser section. On increasing the input power level at the evaporator, the vapor temperature will increase. The vapor pressure will increase rapidly for a very small increase of temperature, causing the gas front to move toward the gas reservoir, thus exposing more condensing surface. Therefore, increasing heat load causes the thermal conductance to increase, which in turn minimizes the pipe temperature change. A cold reservoir VCHP without a wick in the reservoir was shown by the early workers to be troubled by vapor diffusion into the reservoir, followed by condensation. To enable the condensate to be removed, a wicked reservoir is necessary.

The reservoir temperature may be allowed to float or be controlled by a feedback system. A temperature sensor, electronic controller, and a heated reservoir are used to adjust the position of the gas–vapor interface such that the evaporator temperature remains constant. The reservoir is heated to increase the specific volume of the noncondensable gas within it or cooled to decrease it. Note that the change in saturation pressure of the vapor in a wicked reservoir adds to changing the specific volume of the noncondensable. Thus, noncondensable gas is driven out of the reservoir into the condenser or vice versa to achieve correspondence between the evaporator temperature and the control set point by adjusting the active condenser length.

### Startup Transient

When power is applied to the evaporator from a cold start, as the heat warms the inner wall, ammonia vapor evaporates from the liquid in the grooves. The loss of liquid in the grooves creates more curvature of the meniscus, and thus creates a greater pressure difference across the meniscus. Since the pressure in the vapor passages does not vary much along the length of the pipe, there is a higher pressure in the condenser liquid than in the evaporator liquid, and liquid is driven (or drawn) from the condenser into and along the slab wick to the evaporator grooves. Meanwhile, the vapor entering the vapor space sweeps down the length of the tube and condenses on any cold surface. Noncondensable gas is swept past the region where appreciable condensation occurs. Thus, the total

Received March 27, 1995; presented as Paper 95-2137 at the AIAA 30th Thermophysics Conference, San Diego, CA, June 19–22, 1995; revision received Aug. 17, 1995; accepted for publication Aug. 17, 1995. 

*Vice President/Advanced Development, P.O. Box 6034. Member AIAA.

†Professor Emeritus, Department of Mechanical and Aerospace Engineering. Fellow AIAA.

pressure in the pipe becomes the vapor pressure of the ammonia in equilibrium with the wetted warm evaporator wall. The axial region where the composition of the vapor phase changes from pure ammonia vapor to a mixture of gas and ammonia in equilibrium with the cold wall is termed the gas front. Early during the startup transient the gas front is established at the evaporator end of the adiabatic section. As more time passes, the gas front moves slowly through the adiabatic section as the condensation warms the heat pipe wall. Finally the gas front moves down the condenser until a sufficient gas-free length of condenser is attained to dissipate the power to the condenser sink. At this point steady state is achieved.

**Variable Conductance Heat Pipe Modeling**

Edwards and Marcus[5] considered axial heat conduction through the pipe wall to predict heat and mass transfer capability along the gas-controlled heat pipe. Both experimental and computational results showed that axial heat conduction is of much greater importance than axial mass diffusion. With a lower thermal conductivity of the pipe material, a sharper gas–vapor front was noted. The model assumed a one-dimensional diffuse front with uniform gas concentration across the vapor core, which is not entirely satisfactory because radial mass diffusion in addition to axial diffusion causes gas to accumulate at the vapor–liquid interface, and thus, retards the condensation of vapor.

In an analysis prior to this, it has been assumed that axial conduction was negligible and that there exists a sharp interface between the vapor and noncondensable gas. This flat-front assumption was inconsistent with experimental observations that showed that the decrease in vapor concentration occurs smoothly over an appreciable length of the heat pipe. The analysis was formulated based on a one-dimensional model taking into account the axial diffusion, but it neglected the effects of the gas distribution due to radial diffusion, whereas Marcus[6] ignored diffusion altogether.

Hijikata et al.[7] and Tien and Chen[8] demonstrated cases where an adequate description of the gas effect requires a two-dimensional analysis accounting for both axial and radial diffusion of gas mass. Peterson and Tien[9] and Chang and Yu[10] have presented an analytical solution of a steady-state two-dimensional problem of simultaneous heat and mass transfer at the presence of diffusion within a gas-loaded heat pipe and have revealed the importance of the radial dependence of the noncondensable gas distribution on the condenser performance of the heat pipe. The axial distribution function coupled with the liquid–vapor interface temperature was established by a local overall energy balance across the wick/shell structure of the condenser section, and the liquid–vapor interface mole fractions based on local saturation equilibrium of the condensing vapor. Mass diffusion between vapor and gas in the radial direction was shown to have an appreciable effect on the heat transfer in the vapor–gas interface region and on the temperature distribution along the condenser wall.

Bobco[11–13] developed a relatively simple model to calculate evaporator temperature and axial temperature profiles as a function of heat input at the evaporator and environmental conditions. The model used an inhomogeneous one-dimensional fin equation and a mean value approximation to relate the mass of noncondensable gas to the gas front location. The formulation was validated by comparing the experimental results reported by Edwards and Marcus.[5] Bobco claimed that his model provided relatively good predictions of steady-state heat pipe performance despite its neglect of some physical features. It should be noted that neither Edwards and Marcus nor Bobco provided for the gas front changing shape during its movements.

In what follows this article examines the question of how the axial temperature profile changes due to the motion of the gas front during VCHP transients, both analytically and experimentally. A moving-front analysis is then incorporated into an engineering model of transient VCHP performance and comparisons are made of measured behavior and the predictions of the model as depicted in Fig. 1.

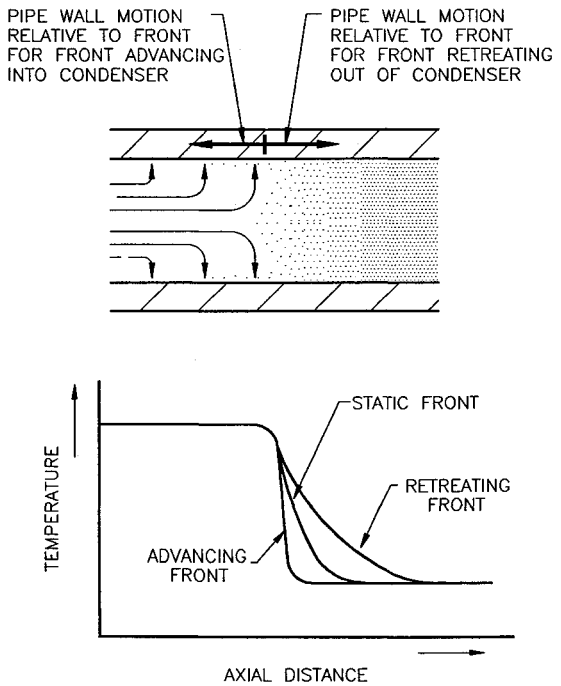


**Fig. 1 Schematic—temperature profile changes among advancing, static, and retreating heat pipe gas fronts.**

## Theory

**Advancing Front**

Consider a heat pipe where the gas front advances at $v$ through the condenser toward the gas reservoir. As the gas retreats it uncovers the condenser wall, which is heated by condensing vapor to $T_e$. Far down the condenser the gas-blocked pipe is at $T_s$. By mathematically transforming the length coordinate to one moving with the front and viewing the heat pipe in that moving coordinate system, the pipe is made to appear to move in the negative $z$ direction at $v$ toward the new origin, which is maintained at $T_e$. Accordingly, the following heat balance applies to an element, fixed in the moving coordinate space, between $z$ and $z + dz$ as shown in Fig. 2. The heat balance expresses the first law of thermodynamics for a steady flow process. The first law expresses the rise in enthalpy of the flowing heat pipe due to the net heat conduction into the element:

$$vA\rho c[T(z) - T(z + dz)] = -kA\left(\frac{dT}{dz}\right)_z + kA\left(\frac{dT}{dz}\right)_{Z+dZ} - UP\,dz(T - T_s) \quad (1)$$

$$kA\left(\frac{d^2T}{dz^2}\right) + vA\rho c\left(\frac{dT}{dz}\right) - UP(T - T_s) = 0 \quad (2)$$

In this heat balance for an element in the gas-blocked region ahead of the advancing front, latent heat transport is neglected compared to axial conduction following the reasoning of Edwards and Marcus.[5] The axial conduction and heat capacity terms are composite values summed over the heat pipe wall, wick, and saddle.

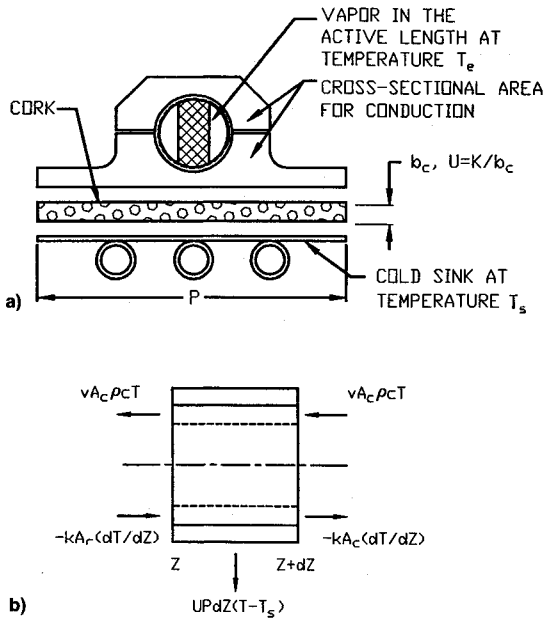


**Fig. 2 Axial conduction model for the condenser: a) cross section and b) heat balance terms, Eq. (1) (note velocity appears in the front-based coordinate system in the sense shown for an advancing front).**

This governing differential equation is subject to

$$z = 0 \qquad T = T_e \tag{3}$$

$$z \to \infty \qquad T = T_s \tag{4}$$

The governing differential equation can be made homogeneous by introducing

$$\Theta = (T - T_s)/(T_e - T_s) \tag{5}$$

and a length scale based upon conduction can be defined

$$UPL^2/kA \equiv 1, \qquad L = (kA/UP)^{1/2} \tag{6}$$

The length scale is made dimensionless in terms of

$$z^* = z/L \tag{7}$$

The remaining parameter in the governing equation is a dimensionless grouping commonly called Peclet number (but here the properties $\rho$, $c$, and $k$ are those of the pipe wall composite, not the fluid):

$$Pe = vL\rho c/k = vL/\alpha \tag{8}$$

Thus, the governing differential equation becomes

$$\frac{d^2\Theta}{dz^{*2}} + Pe\frac{d\Theta}{dz^*} - \Theta = 0 \tag{9}$$

Subject to

$$\Theta = 1 \quad \text{at} \quad z^* = 0 \tag{10}$$

$$\Theta = 0 \quad \text{at} \quad z^* \to \infty \tag{11}$$

The eigenvalues are the roots of the characteristic equation to Eq. (9)

$$m^2 + Pe\, m - 1 = 0 \tag{12}$$

$$m = [-Pe \pm (Pe^2 + 4)^{1/2}]/2 \tag{13}$$

In view of boundary condition Eq. (11) the positive root requires a zero coefficient, and in view of Eq. (10) the negative root takes a unit coefficient so that the solution is

$$\Theta = \exp\{[-(1 + Pe^2/4)^{1/2} - Pe/2]z^*\} \tag{14}$$

This result shows plainly that the front shape is an exponential

$$\Theta = \exp(-|m|z/L) \tag{15}$$

where

$$|m| = (1 + Pe^2/4)^{1/2} + Pe/2 \tag{16}$$

and, since $|m|$ is greater than one and grows with velocity $v$, the front width $L/|m|$ reduces (the front steepens) as the advancing velocity increases.

Because the temperature gradient steepens as the advancing front velocity increases, the heat flux out of the active section does also:

$$Q = -kA\left(\frac{dT}{dz}\right)_{Z=0} = -\left[kA\frac{(T_e - T_s)}{L}\right]\left(\frac{d\Theta}{dz^*}\right)_{Z^*=0} \tag{17}$$

$$Q = +kA(T_e - T_s)|m|/L \tag{18}$$

The heat flux grows as $|m|$ increases past one. A final observation is that if Peclet number were to get much greater than two, the multiplier $|m|$ goes to Peclet

$$|m| \to Pe \quad \text{as} \quad Pe \to \infty \tag{19}$$

$$Q \to \rho cvA(T_e - T_s) \quad \text{as} \quad Pe \to \infty \tag{20}$$

For small Peclet number

$$|m| \doteq 1 + Pe/2 \quad \text{as} \quad Pe \to 0 \tag{21}$$

**Static Front**

For the static front $v = 0$, and the previous results pertain with $Pe = 0$ and $|m| = 1$.

**Retreating Front**

As a front retreats at $v$ toward the evaporator it appears relative to the moving front that hot pipe at $T_e$ flows past the origin. It is merely necessary to reverse the sign upon $v$ in Eq. (2) and upon Peclet number in Eq. (9). Thus, the active eigenvalue is

$$m = -(Pe^2 + 4)^{1/2}/2 + Pe/2 \tag{22}$$

and its absolute value is

$$|m| = (1 + Pe^2/4)^{1/2} - Pe/2 \tag{23}$$

Here, Peclet number is as defined in Eq. (8), with $v$ understood to be its absolute value. Again, the shape of the front is an exponential with a decay length of $L/|m|$, but now, as $Pe$ increases, the magnitude $|m|$ decreases, and the decay length increases.

Equation (18) still serves to give the heat flow. Now, as Peclet number increases, the eigenvalue multiplier $|m|$ decreases according to Eq. (23) and goes to zero as $Pe$ goes to infinity. When $Pe$ is small, Eq. (23) reduces to

$$|m| \doteq 1 - Pe/2 \quad \text{as} \quad Pe \to 0 \tag{24}$$

much like Eq. (21), but with the sign on $Pe$ reversed.

Whether or not the movement of the gas front affects the temperature profile and the heat flow from the active section

to the gas-blocked section depends upon the magnitude of Peclet number. When Peclet number (divided by two) is small compared to one, the effects are small. When the velocity of the gas front is known, Peclet number is computed according to Eq. (8) using the length scale defined in Eq. (6). When Peclet number is not negligible, Eq. (16) or (23) is used, depending upon whether the front is advancing or retreating, respectively, and the shape of the gas-blocked temperature profile [Eq. (15)] or the heat flow from the active section to the inactive section [Eq. (18)] can be found accordingly.

### Heat Balance

The heat balance on the active section of the pipe thus takes the form

$$C\left(\frac{dT_e}{dt}\right) = Q_e - UP(L_e - L_b)(T_e - T_s) - Q \quad (25)$$

where Eq. (18) gives $Q$, and $|m|$ is given by Eq. (16) if the front is advancing, or Eq. (23) if the front is retreating.

**Table 1 Specifications of the test heat pipe**

| |
|---|
| Working fluid, ammonia ($NH_3$) |
| Inert gas, i) mixture of He 19%, Ne 81% |
| ii) 100% Argon |
| Pipe material, stainless steel |
| Wick material, aluminum made by Metex, New Jersey |
| Wick shape, knitted slab wick, 5.1 mm (0.20 in.) thick, 80% porosity |
| Groove size, circumferential grooves, 0.10–0.178 mm (0.007–0.009 in.) deep |
| Groove pitch, 0.25 mm (0.01 in.), 4 grooves per mm (100 grooves per in.) |
| Pipe o.d., 12.7 mm (0.50 in.) diameter |
| Pipe i.d., 11.28 mm (0.444 in.) diameter |
| Overall length, 1.43 m (56.3 in.) |
| Evaporator length, 0.508 m (20.0 in.) |
| Condenser length, 0.508 m (20.0 in.) |
| Adiabatic length, 0.203 m (8.0 in.) |
| Reservoir volume, 70 cc (4.21 in.) |
| Reservoir wick, 0.63-mm-thick, 304 stainless steel felt with 80 porosity |
| Fluid inventory, 50 g |
| Gas amount, $2.182 \times 10^{-5}$ K mol (489 standard cubic centimeter) |

## Apparatus

### Heat Pipe Assembly

The experimental setup consisted of a 1.43-m- (56.3-in.-) long ammonia variable conductance heat pipe with an evaporator heating saddle, a condenser cooling saddle, a cooling system, a reservoir cooling coil with insulation, and a fill tube with valves attached as shown in Fig. 3. The specifications of the heat pipe that were used are shown in Table 1, and the cross sections of the evaporator and condenser are shown in Figs. 4 and 5, respectively. The heat pipe was supplied by TRW Space and Technology Group, Redondo Beach, California. The pipe was a 304 stainless steel tube, 12.7 mm (0.50 in.) in o.d., containing within it a uniform slab wick of aluminum mesh that provides for the axial transport of the ammonia working fluid. The inside surface of the pipe was grooved at 4 grooves per mm (100 grooves per in.) to provide circumferential wetting of the inside surface with liquid drawn by the grooves from the wick.

The reservoir is made from a 0.8-mm- (0.032-in.-) thick stainless steel sheet formed into a short cylinder with hemispherical end caps with the dimensions indicated in Fig. 3. A 0.63-mm- (0.025-in.-) thick stainless steel felt wick is spot-welded to the inner surface of the reservoir. A fill tube, 3.2 mm (0.125 in.) in o.d., with two needle valves are attached to the far end of the reservoir to allow reprocessing and provide access for internal pressure measurements. The reservoir provides volume to contain the noncondensable control gas saturated with ammonia vapor in equilibrium with the wet reservoir wick.

The heat pipe was clamped between saddles as shown in Figs. 4 and 5. At the evaporator, the flat of the saddles was bonded to flexible heaters that have Inconel electrical heating elements in printed circuit form laminated between two layers of 50-$\mu$m- (0.002-in.-) thick Kapton®/FEP (Du Pont Polyimide Film) for electrical insulation. The heaters were supplied by Tayco Engineering, Inc., Cypress, California. At the condenser, the flat of the saddles was clamped to a copper cooling plate with a 3.2-mm- (0.125-in.-) thick cork sheet to provide a desired amount of thermal resistance. The cooling plate has a 0.76-m- (30-in.-) long copper tubing 6.4 mm (0.25 in.) in o.d. brazed to it. Two 254-mm- (10-in.-) long cooling plates connected together were installed along the 508-mm-

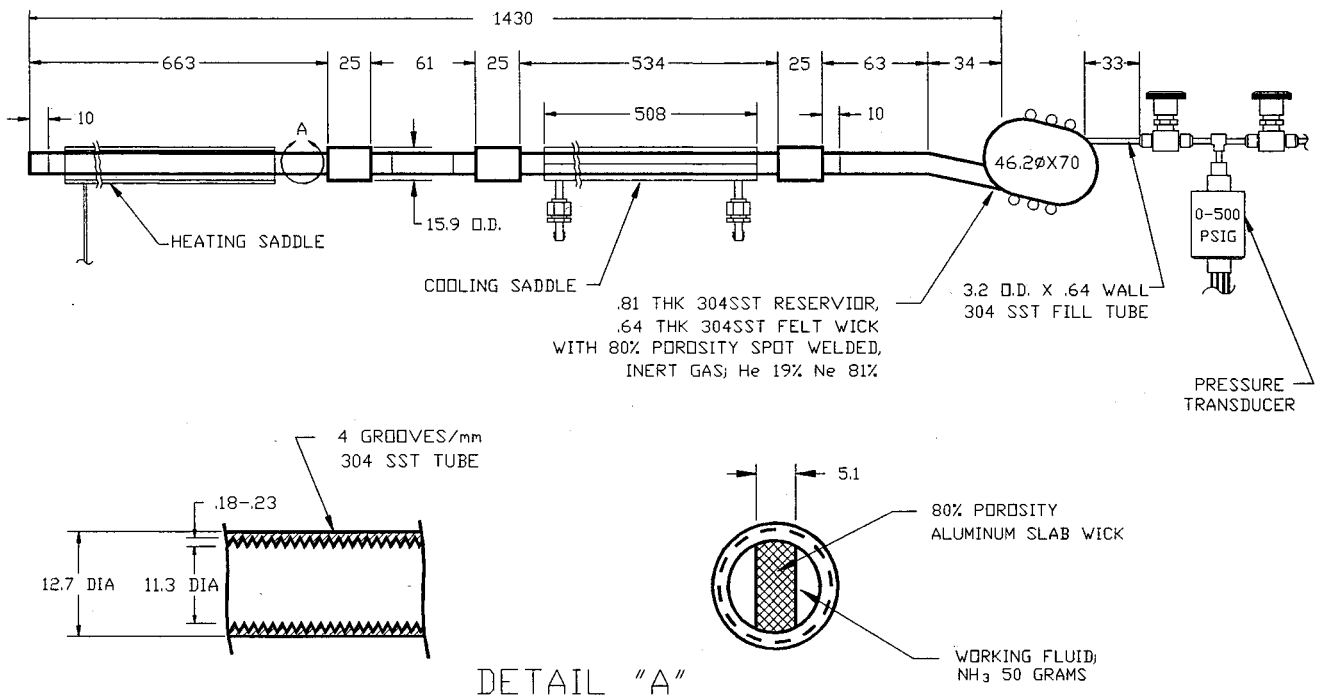


**Fig. 3 Test unit—ammonia variable conductance heat pipe assembly (note all dimensions are shown in millimeters).**

(20-in.-) long condenser section. The coolant circulating through the cooling plate tubing passed through a heater–cooler, Neslab Model Coolflow-33.

Another Tayco flexible heater was bonded to the surface of the gas reservoir that was then wrapped with a cooling coil to provide both heating and cooling as required. The gas reservoir also had an option of being insulated with preformed 50-mm- (2-in.-) thick polyurethane foam.

### Instrumentation

A schematic diagram of the pressure and temperature monitoring setups is depicted in Fig. 6. A pressure transducer, model TJE/708-18 (Sensotec, Columbus, Ohio), which has a measurement range from 0 to 500 psig, was installed at the end of the fill tube to monitor internal pressure. The output from the pressure transducer is connected to a data acquisition and control system, model HP 3497A (Hewlett Packard) through an amplifier, model 563 F (Ectron, San Diego, California). Twenty thermocouples, 30 AWG copper/constantan type T, were located at the saddle-pipe interface in the condenser section at a 1-in. pitch to determine the temperature distribution along the condenser and to locate the gas front position. Additional 10 thermocouples were attached at various spots along the heat pipe as shown in Fig. 6. All 30 thermocouples were connected to the data acquisition and control system, model HP 3497A, and a multimeter, model HP 3455A.

A controlling and monitoring computer, HP 9836, was interfaced with the HP 3497A data acquisition and control system. The input power level of the heaters was manually controlled with an adjustable dc power supply or ac variac, and times and durations of the power applications were controlled by the controlling computer. A separate constant-voltage power supply, model LZD-22 (Lambda, Melville, New York) was used to promote stability of the pressure transducer amplifier.

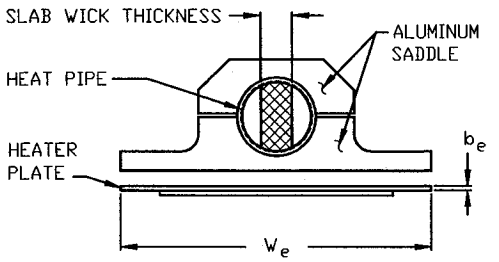


**Fig. 4 Cross section of the heat pipe evaporator.**

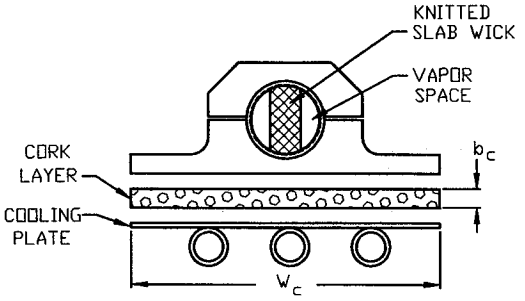


**Fig. 5 Cross section of the heat pipe condenser.**

### Procedure

To investigate heat pipe performances under steady-state or transient conditions, the monitoring computer was programmed in such a way that output data from the data acquisition and control system were recorded in a data storage disk. At each thermocouple location, three successive readings were taken and the midpoint value was recorded. This method was used to minimize any possible errors caused by the internal switching within the data acquisition equipment.

Experiments were preceded by turning on the condenser coolant flow. The coolant temperature was monitored on the surface of the inlet tube at the condenser cooling plate and was kept constant throughout all of the runs within 1.0 K (1.8°F) by the coolflow-33 heater–cooler. A desired input power was applied constantly to the evaporator with one of its heaters and the second heater was operated with or without on–off intervals, depending on the type of run. The pressures and temperatures along the length of the heat pipe were recorded for the period of the test at preset intervals. Switching of heater power was performed through a relay multiplexer

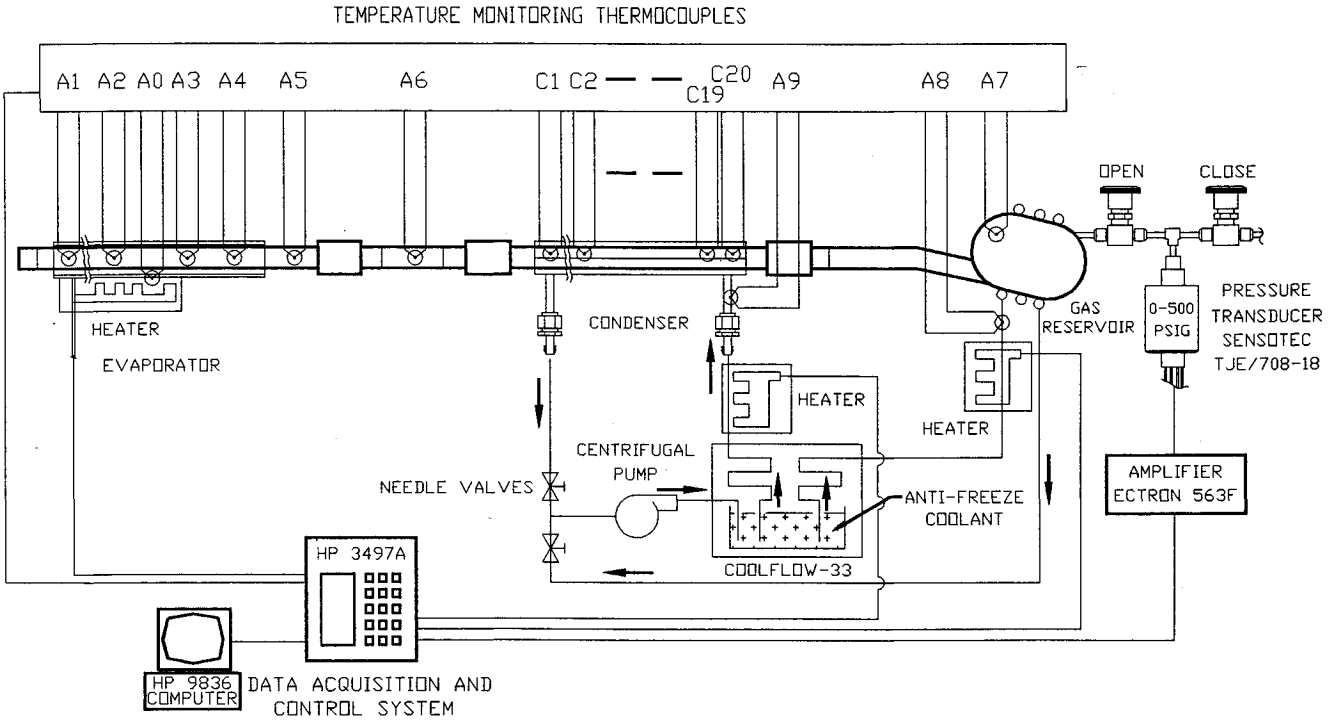


**Fig. 6 Pressure and temperature monitoring setup—VCHP assembly.**

within the data acquisition system and controlled by the computer program.

**Startup Procedure**

The axial temperature profiles along the heat pipe at a preset time interval of 120 s during the startup transient condition were recorded. The data acquisition system and the controlling computer were turned on when the heat pipe was at a cold condition, followed by the application of a constant input power to the evaporator heater until a quasi-steady-state was achieved [temperatures changing less than 0.01 K (0.02°F) per min]. The startup transients were completed in about 30 min.

## Results

Figures 7–9 show experimentally measured axial temperature profiles during startup. For comparison, experimental steady-state temperature profiles are shown in Fig. 10. The steepness or narrowness of the gas-front temperature profiles early in the transient compared to the spread in the steady-state profiles is readily apparent. For example, at 10 min after startup in Fig. 7, the negative slope is approximately 164 K/m (7.5°F/in.) compared to approximately 111 K/m (5.1°F/in.)

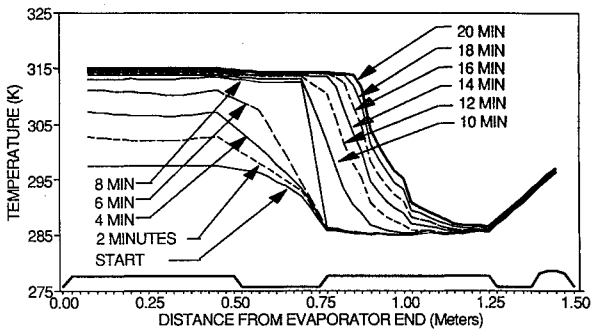


**Fig. 7 Measured axial wall temperature profiles with a step–input power of 30 W.**

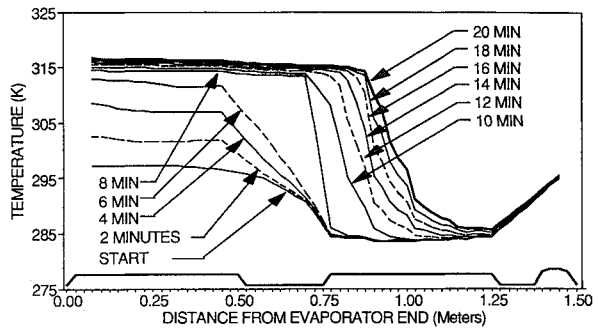


**Fig. 8 Measured axial wall temperature profiles with a step–input power of 40 W.**

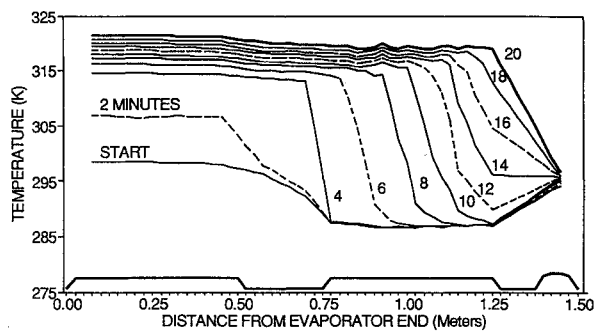


**Fig. 9 Measured axial wall temperature profiles with a step–input power of 70 W.**

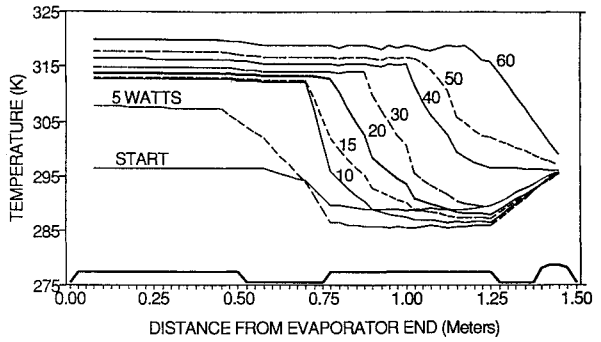


**Fig. 10 Steady-state axial temperature profiles for various input powers.**

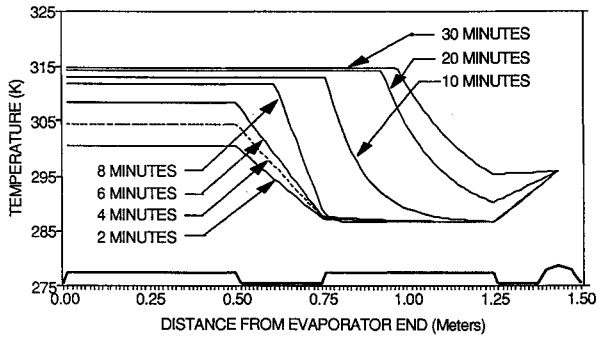


**Fig. 11 Computed axial wall temperature profiles with a step–input power of 30 W.**

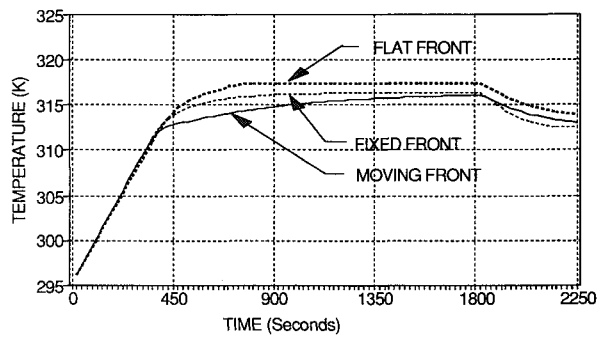


**Fig. 12 Comparison of computed transient evaporator temperatures for flat-front, fixed-front, and moving-front models for an input power of 40 W.**

at steady state. Qualitatively, this steepening of the advancing gas front compared to the static gas front is exactly the behavior predicted by the moving-front theory. Quantitatively, the computer model based upon the theory shows in Fig. 11, 166 K/m (7.6°F/in.) for the advancing front 10 min into the transient and 109 K/m (5.0°F/in.) for the static front 30 min after time zero.

Shown in Fig. 12 is a comparison of the analytically computed evaporator temperature during startup. Shown are predictions for a flat-front, a fixed-front, and a moving-front model. A flat-front model, where the axial thermal conductance is not considered, shows the highest evaporator temperature, unless the gas inventory is adjusted downwards. In a fixed-front model, where the vapor velocity is set to zero in computing the axial conduction past the front, the evaporator temperature converges to the same temperature as the moving front model, once the front has stopped moving. The largest difference in the static- and moving-front models occurs when the gas front emerges from the adiabatic section and moves the fastest into the condenser. It is at this time that the slopes of the evaporator temperature vs time curves

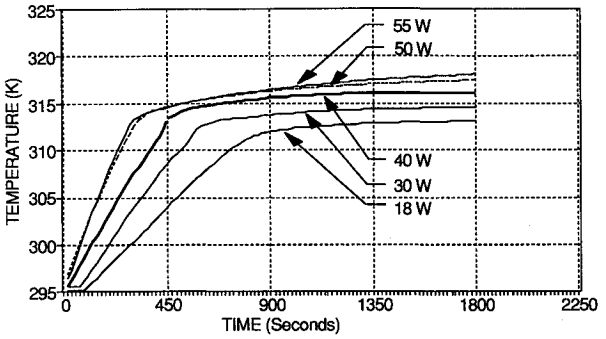


**Fig. 13 Measured evaporator temperatures during startup transient for various input powers.**

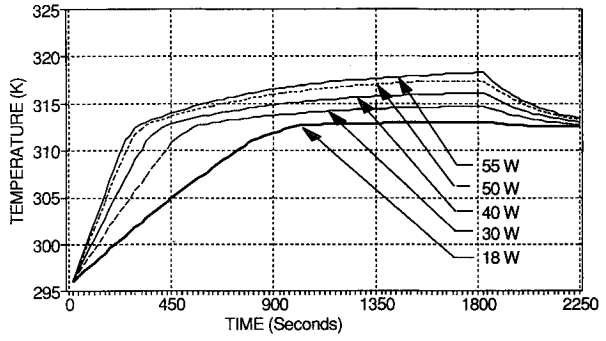


**Fig. 14 Computed evaporator temperatures during the startup transient for various input powers.**

diverge the most. Rates of evaporator temperature change after 30 min are indicated by the following analysis:

| | | |
|---|---|---|
| Flat-front model | = | $0.01 \times 10^{-3}$ K/s |
| Fixed-front model | = | $0.36 \times 10^{-3}$ K/s |
| Moving-front model | = | $2.23 \times 10^{-3}$ K/s |

In comparison, the experimental value taken from Fig. 13 is $2.27 \times 10^{-3}$ K/s in excellent agreement with the moving-front model. Figure 14 shows the computed startup responses corresponding to the experimental results in Fig. 13.

The analytical/numerical results match the behavior of the experimental data shown in Figs. 13 and 14 fairly well. The most notable discrepancy occurs at the transition point where the gas front enters the condenser section from the adiabatic section. At that time the model shows a more abrupt transition than is shown by the data.

Presented here have been selected results from a dissertation[14] by the first author. More extensive results including transient shutdown and cyclic behaviors are presented in the dissertation.

## Acknowledgments

The authors would like to acknowledge David Antoniuk at TRW for his help in arranging the contribution of the test heat pipe. In addition, Charles Taylor, the president of Tayco Engineering, Inc., had the positive vision that enabled the first author to continue this research while working full time.

## References

[1]Grover, G. M., Cotter, T. P., and Erickson, G. F., "Structures of Very High Thermal Conductance," *Journal of Applied Physics*, Vol. 35, No. 6, 1964, pp. 1990, 1991.

[2]Cotter, T. P., "Theory of Heat Pipes," Univ. of California, Los Alamos Scientific Lab., Rept. LA-3246-MS, Los Alamos, NM, March 1965, pp. 1–37.

[3]Wyatt, T., "A Controllable Heat Pipe Experiment for the SE-4 Satellite," Johns Hopkins Univ., Applied Physics Lab., TM APL-SDO-1134, AD 695433, Laurel, MD, March 1965.

[4]Bienert, W. B., Brennan, P. J., and Kirkpatrick, J. P., "Feedback Controlled Variable Conductance Heat Pipes," *Fundamentals of Spacecraft Thermal Design*, edited by J. W. Lucas, Vol. 29, MIT Press, Cambridge, MA, 1972, pp. 463–485.

[5]Edwards, D. K., and Marcus, B. D., "Heat and Mass Transfer in the Vicinity of the Vapor-Gas Front in a Gas-Loaded Heat Pipe," *Journal of Heat Transfer*, Vol. 94, Ser. C, No. 2, 1972, pp. 155–162.

[6]Marcus, B. D., "Theory and Design of Variable Conductance Heat Pipes," NASA CR-2018, April 1972, pp. 1–238.

[7]Hijikata, K., Chen, S. J., and Tien, C. L., "Non-Condensible Gas Effect on Condensation in a Two-Phase Closed Thermosyphons," *International Journal of Heat and Mass Transfer*, Vol. 27, No. 8, 1984, pp. 1319–1325.

[8]Tien, C. L., and Chen, S. J., "Non-Condensable Gases in Heat Pipes," *Pre-Prints II of the 5th International Heat Pipe Conference* International Heat Pipe Conf. Committee, Tsukuba, Japan, 1984, pp. 2–6.

[9]Peterson, P. F., and Tien, C. L., "Numerical and Analytical Solutions for Two-Dimensional Gas Distribution in Gas-Loaded Heat Pipes," *Journal of Heat Transfer*, Vol. 111, 1989, pp. 598–604.

[10]Chang, W. S., and Yu, J. S., "A Note on the Gas Distribution in a Cylindrical Gas-Loaded Heat Pipe," *Journal of Heat Transfer*, Vol. 112, Aug. 1990, pp. 779–781.

[11]Bobco, R. P., "Variable Conductance Heat Pipes: A First Order Model," *Journal of Thermophysics and Heat Transfer*, Vol. 1, No. 1, 1987, pp. 35–42.

[12]Bobco, R. P., "An Extended Model for Variable Conductance Heat Pipe (VCHP) Analysis : Zero-to-Full Heat Loads," AIAA Paper 87-1614, June 1987.

[13]Bobco, R. P., "VCHP Performance Prediction: Comparison of First-Order and Flat Front Models," *Journal of Thermophysics and Heat Transfer*, Vol. 3, No. 4, 1989, pp. 401–405.

[14]Chung, J. H., "Investigation of Transient Behavior in a Gas Controlled Ammonia Heat Pipe," Ph.D. Dissertation, Univ. of California, Irvine, CA, 1994.